ISSN 1573-160X, *PHYSICAL OCEANOGRAPHY*, Vol. 31, Iss. 2, pp. 161-177 (2024)

published in *Morskoy Gidrofizicheskiy Zhurnal*, 2024, Vol. 40, Iss. 2, pp. 180–197

Original article

Generation of Vertical Fine Structure by Internal Waves on a Shear Flow

A. A. Slepyshev ✉, **N. O. Ankudinov**

Marine Hydrophysical Institute of RAS, Sevastopol, Russian Federation
✉ *slep55@mail.ru*

Abstract
Purpose. The work is purposed at studying the wave mechanism of fine structure generation, as well as determining the vertical wave fluxes of mass.
Methods and Results. In contrast to the previously used mechanism of forming a fine structure by internal waves due to breaking, a new approach based on determining the vertical wave fluxes of mass in the field of an inertia-gravity internal wave without breaking is proposed. The inertia-gravity internal waves on the Black Sea northwestern shelf are considered on a flow with a vertical velocity shift. The flow is assumed to be geostrophically balanced with the vertical velocity shifts compensated by a horizontal density gradient. The *f*-plane approximation is used. Thus, the classical scheme for describing a wave field by the hydrodynamic equations is applicable with regard to the nonlinear effects. A weakly nonlinear approach is used. In the linear approximation, the eigenfunction and the dispersion relation are found by solving numerically the boundary value problem which determines the vertical structure of a mode in the presence of an average flow. In this case, the wave frequency is of a complex character since the coefficients in the differential equation of the specified boundary value problem are complex. Depending on the wave period and the mode number, either weak attenuation of a wave or its weak amplification is possible. The eigenfunction of internal waves is also complex. Therefore, the vertical wave fluxes of mass and the vertical component of the Stokes drift velocity are nonzero and lead to the generation of vertical fine structure which is irreversible.
Conclusions. In the presence of a two-dimensional shear flow, taking into account the horizontal inhomogeneity of the average density field enhances the effect of generation of a vertical fine structure by the inertia-gravity internal waves. The vertical wave fluxes of mass also increase. The indicated fluxes and generated fine structure for the waves of different frequencies are close and the effect is enhanced in the presence of the waves of different frequencies.

Keywords: internal waves, fine structure, Stokes drift

Acknowledgments: The study was carried out within the framework of the theme of state assignment FNNN-2021-0004.

For citation: Slepyshev, A.A. and Ankudinov, N.O., 2024. Generation of Vertical Fine Structure by Internal Waves on a Shear Flow. *Physical Oceanography*, 31(1), pp. 161-177.

Introduction

Fine structure of a liquid medium is a very interesting object studied both theoretically and experimentally under laboratory conditions. Structures amenable to detailed experimental study and theoretical analysis [1, 2] arise when solids move in a liquid. No less interesting structures [3] appear when a liquid drop falls onto a liquid. Such structures can explain the processes in the sea surface layer during precipitation.

The fine structure of hydrophysical fields was discovered almost half a century ago owing to the creation of high-resolution sounding equipment. Indeed, no one had

imagined before its discovery that temperature and salinity vertical profiles on small spatial scales were very variable. This variability was initially thought [1] [4] to be due to small-scale turbulence, also not fully understood object. But then it turned out that not only turbulence was responsible for the fine structure generation as the kinematic effect of internal waves also gave a fine structure in measurements [5, 6]. However, this was not a long-lived structure since the kinematic effect disappeared after the wave train passage.

Double diffusion provided a mechanism for vertical stratification of temperature and salinity profiles in the ocean [2] [7–10]. The formation of convective cells in the form of salt fingers [11–14] is possible if temperature and salinity decrease with depth. They differ markedly from the surrounding liquid layers in terms of characteristic gradients, i.e. a structure appears with alternating thin stratified layers and quasi-homogeneous ones. This is actually the fine structure. Such conditions are very typical for the World Ocean and approximately 70% of its column is subject to such stratification [2]. Double diffusion takes place when temperature and salinity increase with depth [15, 16]. Geothermal heat sources at the bottom contribute to this process. Double diffusion can lead to the formation of step structures which have been repeatedly observed in field experiments [17, 18]. Intrusive layering with mutual penetration of waters with different T, S-characteristics [19–21] is possible in the area of fronts. Intrusions are possible due to internal wave breaking at the shelf edge in the continental slope area [22].

It should be noted that such conditions are not always realized and this phenomenon is more exotic than widespread in inland seas far from fronts. The fine structure still exists and can be explained by other mechanisms which, of course, also work in the open ocean. The internal waves breaking and hydrodynamic instability of flows is the mechanism that has been proposed to explain the fine structure formation [23–26]. However, it turned out that internal waves do not necessarily have to break in order to generate a fine structure. The wave field is intermittent, and internal waves often propagate as wave trains [27]. Due to nonlinearity, trains of internal waves produce small corrections to the flow density and velocity [28] with a horizontal scale equal to the train envelope scale, and the vertical scale is determined by relation c_g / N, where c_g is group velocity of train and N is Brunt–Väisälä frequency. However, these corrections are proportional to the square of the current wave amplitude and disappear after the wave train passage.

The waves attenuate and form boundary layers in the vicinity of the boundaries [29, 30] in a dissipative medium when viscosity and diffusion are taken into account. A beam of three-dimensional internal waves is reflected from the layer where wave and buoyancy frequencies coincide and the reflection occurs with energy losses [31] which can amount to several percentage points. Internal

[1] Gibson, C.H., 1980. Fossil Temperature, Salinity, and Vorticity Turbulence in the Ocean. In: J. C. J. Nihoul, ed., 1980. *Marine Turbulence*. Amsterdam: Elsevier Publising Co., pp. 221-257. https://doi.org/10.1016/S0422-9894(08)71223-6

[2] Fedorov, K.N., 1978. *The Thermohaline Finestructure of the Ocean*. Oxford; New York: Pergamon Press, 170 p.

boundary layers are formed at discontinuities in the buoyancy frequency or its derivatives in the beam of internal waves with a reflected beam also present [31]. Boundary layers have split density and velocity scales. These boundary flows generate fine structure of the periodic flow.

Internal waves attenuate [32, 33] when turbulent viscosity and diffusion are taken into account. Vertical wave fluxes of heat, salt and momentum are nonzero and lead to the formation of an already irreversible fine structure [34–38]. However, not only consideration of turbulent viscosity and diffusion leads to the vertical fine structure generation. When taking into account the Earth rotation and inhomogeneous average flows, vertical wave fluxes of heat, salt and mass are nonzero even when turbulent viscosity and diffusion are not taken into account and result in formation of a vertical fine structure [39]. Vertical wave momentum fluxes are also nonzero [40–44]. However, the horizontal average density gradient which is always present in a geostrophically balanced flow was not considered in [39]. It was assumed that the horizontal scale of wave is much smaller than the scale of the average density field inhomogeneity. We take into account the horizontal gradient of average density and perform a comparison with the results for a homogeneous case in the present work. In [39], the boundary value problem for the vertical velocity amplitude is solved by the perturbation method with the introduction of small parameter $\varepsilon = V_0 / (H \cdot \omega)$, where V_0 is characteristic flow velocity, H is depth and ω is wave frequency. However, this parameter is not always small and in this work the boundary value problem for the amplitude of internal wave vertical velocity is solved numerically using the implicit Adams scheme of the third order accuracy [40, 42].

Problem statement

Free internal waves are considered in the Boussinesq approximation with regard to the Earth rotation and the average two-dimensional vertically inhomogeneous flow in a horizontal infinite basin of constant depth [34–44]. The *f*-plane approximation is used. Horizontal gradients of average density are found from geostrophic relations [3] and expressed through vertical shifts of flow velocity components, as in [45]. The system of hydrodynamic equations for wave disturbances in the Boussinesq approximation is as follows:

$$\frac{D\mathbf{u}}{Dt} + 2\left[\mathbf{\Omega}_{\perp} \times \mathbf{u}\right] + u_3 \frac{d\mathbf{U}^0}{dx_3} = -\frac{1}{\bar{\rho}_0}\nabla P + \mathbf{g}\frac{\rho}{\bar{\rho}_0}, \tag{1}$$

$$\frac{D\rho}{Dt} + (\mathbf{u}\nabla)\rho_0 = 0, \tag{2}$$

$$div\mathbf{u} = 0, \tag{3}$$

[3] Kamenkovich, V.M., 1977. *Fundamentals of Ocean Dynamics*. Amsterdam; New York: Elsevier Scientific Pub. Co., 249 p.

where $\mathbf{u}(u_1, u_2, u_3)$ is vector of flow velocity wave disturbances; ρ, P are density and pressure wave disturbances; ρ_0 is unperturbed average density; x_3 axis is directed opposite to the gravitational acceleration vector $\mathbf{g}$; $\mathbf{\Omega}_\perp$ is vector of projection of the Earth rotation angular velocity onto the axis x_3; $\mathbf{U}^0$ $\left(U_1^0(x_3), U_2^0(x_3), 0\right)$ is vector of average flow velocity; operator $\frac{D}{Dt}$ has form $\frac{D}{Dt} = \frac{\partial}{\partial t} + \left((\mathbf{u} + \mathbf{U}^0)\nabla\right)$.

From the "thermal wind" relations [3] [45], the components of average density horizontal gradient are expressed through vertical shifts in the flow velocity as follows:

$$\frac{\partial \rho_0}{\partial x_1} = -\frac{\overline{\rho}_0 f}{g}\frac{dU_2^0}{dx_3}, \tag{4}$$

$$\frac{\partial \rho_0}{\partial x_2} = \frac{\overline{\rho}_0 f}{g}\frac{dU_1^0}{dx_3}, \tag{5}$$

where $f = 2\left(\mathbf{\Omega}_\perp \mathbf{e}_3\right) = 2\Omega_E \sin\varphi$ is Coriolis parameter, $\mathbf{e_3}$ is unit vector of x_3 axis, Ω_E is angular velocity of the Earth rotation, φ is latitude.

After substituting relations (4), (5) into equation (2), the latter becomes as follows:

$$\frac{D\rho}{Dt} - u_1\frac{\overline{\rho}_0 f}{g}\frac{dU_2^0}{dx_3} + u_2\frac{\overline{\rho}_0 f}{g}\frac{dU_1^0}{dx_3} + u_3\frac{\partial \rho_0}{\partial x_3} = 0. \tag{6}$$

The boundary condition on the sea surface is the "rigid lid" condition which filters internal waves from surface ones and on the bottom – the impermeability condition [4]:

$$u_3 = 0 \quad \text{at } x_3 = 0, \tag{7}$$

$$u_3 = 0 \quad \text{at } x_3 = -H, \tag{8}$$

where H is sea depth.

Linear approximation. We look for solutions to equations (1), (3), (6) in a linear approximation under the condition of horizontal homogeneity of Brunt–Väisälä frequency on the wave scale in the following form [34–45]:

$$u_i = u_{i0}(x_3)A\mathrm{e}^{i\theta} + \text{c.c.}, \quad i = 1, 2, 3, \tag{9}$$

$$P = P_1(x_3)A\mathrm{e}^{i\theta} + \text{c.c.}, \quad \rho = \rho_1(x_3)A\mathrm{e}^{i\theta} + \text{c.c.}, \tag{10}$$

[4] Miropolsky, Yu.Z., 1981. *Dynamics of Internal Gravitational Waves in the Ocean*. Leningrad: Gidrometeoizdat, 302 p. (in Russian).

where c.c. are complex-conjugate terms; A is amplitude multiplier; $\theta = k x_1 - \omega t$ is wave phase, k is horizontal wavenumber, ω is wave frequency. We assume that the wave propagates along x_1 axis.

Expressions for amplitude functions $u_{10}, u_{20}, \rho_1, P_1$ through u_{30} follow from system (1), (3), (6):

$$u_{10} = \frac{i}{k}\frac{du_{30}}{dx_3}, \qquad \Omega = \omega - k \cdot U_1^0, \tag{11}$$

$$\frac{P_1}{\overline{\rho}_0} = \frac{i}{k}\left[\frac{\Omega}{k}\frac{du_{30}}{dx_3} + \frac{dU_1^0}{dx_3}u_{30} + \frac{f}{\Omega}\left(i\frac{dU_2^0}{dx_3}u_{30} - \frac{f}{k}\frac{d}{dx_3}u_{30}\right)\right],$$

$$u_{20} = \frac{1}{\Omega}\left(\frac{f}{k}\frac{du_{30}}{dx_3} - iu_{30}\frac{dU_2^0}{dx_3}\right). \tag{12}$$

$$\rho_1 = \frac{i}{\Omega}\left[\frac{i}{k}\frac{\overline{\rho}_0 f}{g}\frac{dU_2^0}{dx_3}\frac{du_{30}}{dx_3} - u_{30}\frac{d\rho_0}{dx_3} - \frac{\overline{\rho}_0 f}{g\Omega}\frac{dU_1^0}{dx_3}\left(\frac{f}{k}\frac{du_{30}}{dx_3} - iu_{30}\frac{dU_2^0}{dx_3}\right)\right], \tag{13}$$

where $\Omega = \omega - k \cdot U_0$ is frequency with Doppler shift.

The amplitude function of the vertical velocity component u_{30} satisfies the equation

$$\begin{aligned}&\frac{d^2u_{30}}{dx_3^{\,2}} + k\left[\frac{2if\dfrac{dU_2^0}{dx_3}}{\Omega^2 - f^2} - \frac{2f^2\dfrac{dU_1^0}{dx_3}}{\Omega(\Omega^2 - f^2)}\right]\frac{du_{30}}{dx_3} + \\ &+ku_{30}\left[\frac{k(N^2 - \Omega^2) + \Omega\dfrac{d^2U_1^0}{dx_3^{\,2}} + if\dfrac{d^2U_2^0}{dx_3^{\,2}}}{\Omega^2 - f^2} + \frac{2ifk\dfrac{dU_1^0}{dx_3}\dfrac{dU_2^0}{dx_3}}{\Omega(\Omega^2 - f^2)}\right] = 0,\end{aligned} \tag{14}$$

where $N^2 = -\frac{g}{\overline{\rho}_0}\frac{d\rho_0}{dx_3}$ is squared Brunt–Väisälä frequency.

Boundary conditions for u_{30} are as follows:

$$u_{30}(0) = u_{30}(-H) = 0. \tag{15}$$

Equation (14) has complex coefficients, therefore, generally speaking, its solution is a complex function and boundary value problem (14)–(15) must also have complex values of natural frequencies ω at a fixed wave number [34–43]. Indeed, subsequent calculations reveal that the wave frequency has a small imaginary part. Boundary value problem (14)–(15) was solved analytically in [46, 47] without taking into account the Earth rotation at $f = 0$ on a flow with a constant vertical velocity

gradient at constant Brunt–Väisälä frequency. A solution is obtained in the form of imaginary order modified Bessel functions. The dispersion equation was solved using both asymptotic and numerical methods. It is shown that the flow leads to a noticeable anisotropy of the dispersion curves; in particular, frequency isolines in the plane of horizontal wave numbers can open up. Equation (14) has real coefficients at $f = 0$, so the wave frequency and the eigenfunction of internal waves are real when the Richardson number is larger than $1/4$ [46, 47].

Nonlinear effects. The flow velocities in the Euler $\mathbf{u}$ and Lagrange $\mathbf{u}_L$ representations are related by relation [5] [36, 43] up to second-order terms in wave steepness

$$\mathbf{u}_L = \mathbf{u} + (\int_0^t \mathbf{u}_L d\tau \nabla)\mathbf{u}. \tag{16}$$

Solving this equation by iteration method up to terms quadratic in the wave amplitude, we obtain an expression for the average Lagrangian velocity after averaging over the wave period

$$\overline{\mathbf{u}_L} = \mathbf{U} + \overline{(\int_0^t \mathbf{u} d\tau \nabla)\mathbf{u}}, \tag{17}$$

where vector $\mathbf{U}(U_0, V_0)$ is average flow velocity; $\mathbf{u}$ is field of wave Euler velocities; the overbar means averaging over the wave period. The second term in (17) is the Stokes drift velocity which is determined by the following formula [34, 36, 38, 39, 41–43, 48]:

$$\mathbf{u}_S = \overline{(\int_0^t \mathbf{u} d\tau \nabla)\mathbf{u}}. \tag{18}$$

Vertical component of the Stokes drift velocity is nonzero for the complex frequency [39, 42]:

$$u_{3S} = iA_1 A_1^* \left(\frac{1}{\omega} - \frac{1}{\omega^*} \right) \frac{d}{dx_3} \left(u_{30} u_{30}^* \right), \tag{19}$$

where $A_1 = A\exp(\delta\omega \cdot t)$, $\delta\omega = \mathrm{Im}(\omega)$ is wave frequency imaginary part. Two horizontal components of the Stokes drift velocity are determined by the following formulas:

$$u_{1S} = \frac{A_1 A_1^*}{k} \left[\frac{1}{\omega} \frac{d}{dx_3} \left(u_{30} \frac{du_{30}^*}{dx_3} \right) + \text{c.c.} \right], \tag{20}$$

[5] Dvoryaninov, G.S., 1982. *Effects of Waves in the Boundary Layers of the Atmosphere and Ocean*. Kiev: Naukova Dumka, 176 p. (in Russian).

$$u_{2S} = A_1 A_1^* \left[\frac{1}{\omega \Omega^* k} \frac{du_{30}}{dx_3} \left(if \frac{du_{30}^*}{dx_3} - k \frac{dU_2^0}{dx_3} u_{30}^* \right) + \text{c.c.} \right] -$$

$$- A_1 A_1^* \left\{ \frac{u_{30}^*}{\omega^* \Omega^2} \left[\Omega \left(\frac{du_{30}}{dx_3} \frac{dU_2^0}{dx_3} + \frac{if}{k} \frac{d^2 u_{30}}{dx_3^2} + u_{30} \frac{d^2 U_2^0}{dx_3^2} \right) + k \frac{dU_1^0}{dx_3} \left(u_{30} \frac{dU_2^0}{dx_3} + \frac{if}{k} \frac{du_{30}}{dx_3} \right) \right] \right\} + \text{c.c.} \Bigg\}. \quad (21)$$

We find the vertical wave mass flux taking into account formulas (10), (13) [37, 39]:

$$\overline{\rho u_3} = |A_1|^2 \left\{ \frac{i}{\Omega} \left[\frac{i}{k} \frac{\overline{\rho}_0 f}{g} \frac{dU_2^0}{dx_3} \frac{du_{30}}{dx_3} - u_{30} \frac{d\rho_0}{dx_3} - \frac{\overline{\rho}_0 f}{g\Omega} \frac{dU_1^0}{dx_3} \left(\frac{f}{k} \frac{du_{30}}{dx_3} - i u_{30} \frac{dU_2^0}{dx_3} \right) \right] u_{30}^* + \text{c.c.} \right\}. \quad (22)$$

The equation for a correction to average wave density $\overline{\rho}$ that does not oscillate on a time scale, accurate to terms quadratic in the wave amplitude, has the form:

$$\frac{\partial \overline{\rho}}{\partial t} + U_1^0 \frac{\partial \overline{\rho}}{\partial x_1} + U_2^0 \frac{\partial \overline{\rho}}{\partial x_2} + \frac{\partial \overline{\rho u_1}}{\partial x_1} + \frac{\partial \overline{\rho u_2}}{\partial x_2} + \frac{\partial \overline{\rho u_3}}{\partial x_3} + u_{1S} \frac{\partial \rho_0}{\partial x_1} + u_{2S} \frac{\partial \rho_0}{\partial x_2} + u_{3S} \frac{\partial \rho_0}{\partial x_3} = 0 . \quad (23)$$

Considering relations (4), (5), equation (23) is transformed to the form:

$$\frac{\partial \overline{\rho}}{\partial t} + U_1^0 \frac{\partial \overline{\rho}}{\partial x_1} + U_2^0 \frac{\partial \overline{\rho}}{\partial x_2} + \frac{\partial \overline{\rho u_1}}{\partial x_1} + \frac{\partial \overline{\rho u_2}}{\partial x_2} + \frac{\partial \overline{\rho u_3}}{\partial x_3} - u_{1S} \frac{\overline{\rho}_0 f}{g} \frac{dU_2^0}{dx_3} + u_{2S} \frac{\overline{\rho}_0 f}{g} \frac{dU_1^0}{dx_3} + u_{3S} \frac{\partial \rho_0}{\partial x_3} = 0 . \quad (24)$$

In the horizontally homogeneous case equation (24) takes the form:

$$\frac{\partial \overline{\rho}}{\partial t} + \frac{\partial \overline{\rho u_3}}{\partial x_3} - u_{1S} \frac{\overline{\rho}_0 f}{g} \frac{dU_2^0}{dx_3} + u_{2S} \frac{\overline{\rho}_0 f}{g} \frac{dU_1^0}{dx_3} + u_{3S} \frac{\partial \rho_0}{\partial x_3} = 0 . \quad (25)$$

Integrating equation (25) over time, we obtain:

$$\Delta \overline{\rho} = -\int_0^t \left(\frac{\partial \overline{\rho u_3}}{\partial x_3} - u_{1S} \frac{\overline{\rho}_0 f}{g} \frac{dU_2^0}{dx_3} + u_{2S} \frac{\overline{\rho}_0 f}{g} \frac{dU_1^0}{dx_3} + u_{3S} \frac{\partial \rho_0}{\partial x_3} \right) dt' . \quad (26)$$

Substituting $\overline{\rho u_3}$ from formula (22) and three components of the Stokes drift velocity from formulas (19)–(21) into expression (26), after integration we obtain:

$$\Delta \overline{\rho} = \left[\frac{\partial \overline{\rho u_3}^0}{\partial x_3} - u_{1S}^0 \frac{\overline{\rho}_0 f}{g} \frac{dU_2^0}{dx_3} + u_{2S}^0 \frac{\overline{\rho}_0 f}{g} \frac{dU_1^0}{dx_3} + u_{3S}^0 \frac{\partial \rho_0}{\partial x_3} \right] \cdot \frac{1}{2\delta\omega} \left(1 - e^{2\delta\omega \cdot t} \right), \quad (27)$$

where

$$\overline{\rho u_3}^0 = |A|^2 \left\{ \frac{i}{\Omega} \left[\frac{i}{k} \frac{\overline{\rho}_0 f}{g} \frac{dU_2^0}{dx_3} \frac{du_{30}}{dx_3} - u_{30} \frac{d\rho_0}{dx_3} - \frac{\overline{\rho}_0 f}{g\Omega} \frac{dU_1^0}{dx_3} \left(\frac{f}{k} \frac{du_{30}}{dx_3} - i u_{30} \frac{dU_2^0}{dx_3} \right) \right] u_{30}^* + \text{c.c.} \right\},$$

$$u_{1S}^0 = \frac{|A|^2}{k} \left[\frac{1}{\omega} \frac{d}{dx_3} \left(u_{30} \frac{du_{30}^*}{dx_3} \right) + \text{c.c.} \right], \qquad u_{3S}^0 = i |A|^2 \left(\frac{1}{\omega} - \frac{1}{\omega^*} \right) \frac{d}{dx_3} \left(u_{30} u_{30}^* \right),$$

$$u_{2S}^0 = |A|^2 \left[\frac{1}{\omega \Omega^* k} \frac{du_{30}}{dx_3} \left(if \frac{du_{30}^*}{dx_3} - k \frac{dU_2^0}{dx_3} u_{30}^* \right) + \text{c.c.} \right] -$$

$$- |A|^2 \left\{ \frac{u_{30}^*}{\omega^* \Omega^2} \left[\Omega \left(\frac{du_{30}}{dx_3} \frac{dU_2^0}{dx_3} + \frac{if}{k} \frac{d^2 u_{30}}{dx_3^2} + u_{30} \frac{d^2 U_2^0}{dx_3^2} \right) + k \frac{dU_1^0}{dx_3} \left(u_{30} \frac{dU_2^0}{dx_3} + \frac{if}{k} \frac{du_{30}}{dx_3} \right) \right] + \text{c.c.} \right\}.$$

Correction to density $\Delta\overline{\rho}$ determined by formula (27) is a vertical fine structure generated by an internal wave and irreversible [37, 39]. The specified correction is retained after the wave train passage.

Calculation results

We calculate the vertical fine structure generated by the internal wave using the data from the third stage of the 44th cruise of R/V *Mikhail Lomonosov* at the Black Sea northwestern shelf [6] [34, 35, 39–43].

Fig. 1 shows the time course of temperature isolines obtained by four gradient-distributed temperature sensors.

The instruments were hung from the board of the vessel and located at the following depths: 5–15 m – the first instrument; 15–25 m – the second instrument; 25–35 m – the third instrument; 35–60 m – the fourth instrument (indicated in Fig. 1 by Roman numerals I – IV, respectively).

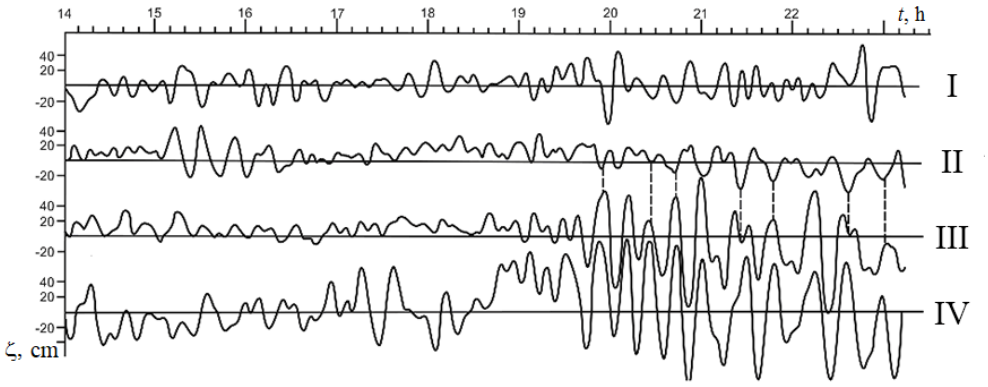

F i g. 1. Dependence of vertical displacements of temperature isolines on time

Figure 1 shows clearly a powerful wave train of 15-minute second-mode internal waves. The maximum amplitude at elevations is 0.5 m.

Figure 2, *a* shows Brunt–Väisälä frequency dependence on the vertical coordinate, and Fig. 2, *b* – dependence on two components of flow velocity.

[6] Panteleev, N.A., 1985. *Report on the Work on the 44th Voyage (3rd Stage) of the NIS Mikhail Lomonosov August 7 – September 15, 1985*. Sevastopol: MHI Academy of Sciences of the Ukrainian SSR. Vol. 1, 135 p. (in Russian).

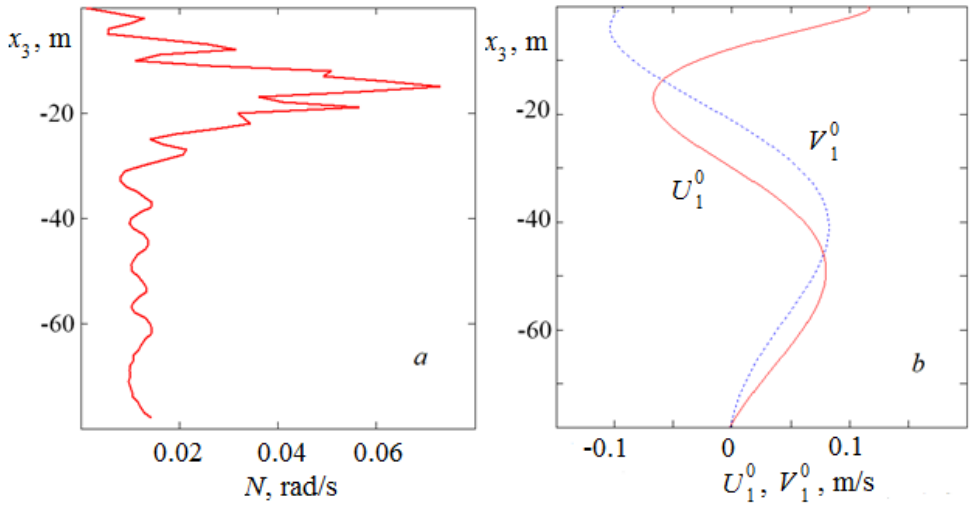

F i g. 2. Dependence of Brunt–Väisälä frequency (*a*) and flow velocity components (*b*) on the vertical coordinate

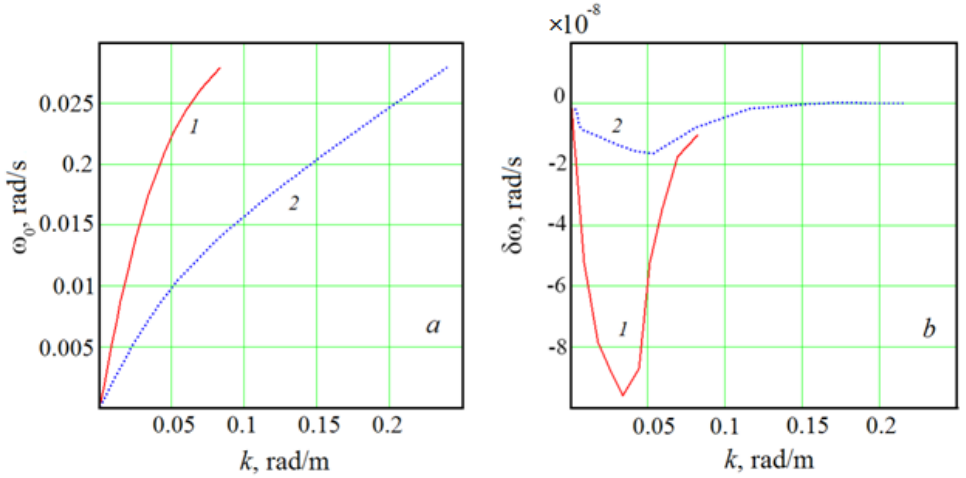

F i g. 3. Dispersion curves (*a*) and graphs of the frequency imaginary part (*b*) of the first (*1*) and second (*2*) modes

The boundary value problem (14), (15) is solved numerically using the implicit Adams scheme of the third order accuracy [34–43]. The shooting method is applied to determine the wave number and frequency imaginary part at a fixed wave period for a given mode of internal waves. The resulting solution is complex, as well as the wave frequency with a small imaginary part. Figure 3, *a* shows the dependence of frequency real part $\omega_0 = \mathrm{Re}(\omega)$ on the wave number for the first two modes. Figure 3, *b* reveals the dependence of the frequency imaginary part on the wave number. The imaginary part of first-mode frequency $\delta\omega = \mathrm{Im}(\omega)$ is negative, i.e. the wave is slightly attenuated.

For the second mode, the imaginary part of the frequency is negative when frequency ω_0 is less than 12 cph; if the frequency is higher, its imaginary part is positive, i.e., weak attenuation in the low-frequency region is replaced by weak amplification in the high-frequency region. The first-mode damping decrement is greater in absolute value than the second-mode damping decrement for a fixed wave number. For 15-minute internal waves of the second mode, the attenuation decrement is equal to $\delta\omega = -1,4 \cdot 10^{-8}$ rad/s, the wavelength is 197 m.

We calculate the vertical component of the Stokes drift velocity using formula (19). Normalizing factor A_1 is found by the known maximum amplitude of 0.5 m vertical displacements. The dependence of the Stokes drift velocity vertical component on the vertical coordinate for the first two modes is demonstrated in Fig. 4, *a*, the wave frequency was 4 cph.

Fig. 4, *b* shows the average density vertical profile.

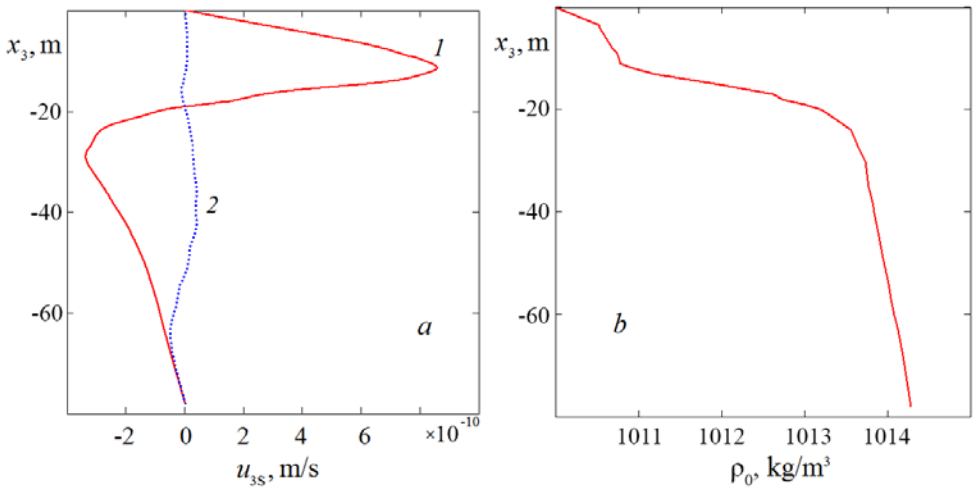

F i g. 4. Dependence of vertical component of the Stokes drift velocity on the vertical coordinate of internal waves of the first (*1*) and second (*2*) modes (*a*); average density profile (*b*)

Fig. 5 shows the profiles of vertical mass flow determined by formula (22) and non-oscillating correction to density (formula (27)) at $t = 9$ h for the first two modes of internal waves with 4 cycle/h frequency at the same maximum amplitude of 0.5 m.

The vertical wave mass flux of the first mode predominates significantly in the upper 40-meter layer, while the wave fluxes of the first and second modes are comparable in absolute value at greater depths. The intensity of the generated vertical fine structure of the density field for the first mode is greater than for the second one at the same maximum wave amplitude.

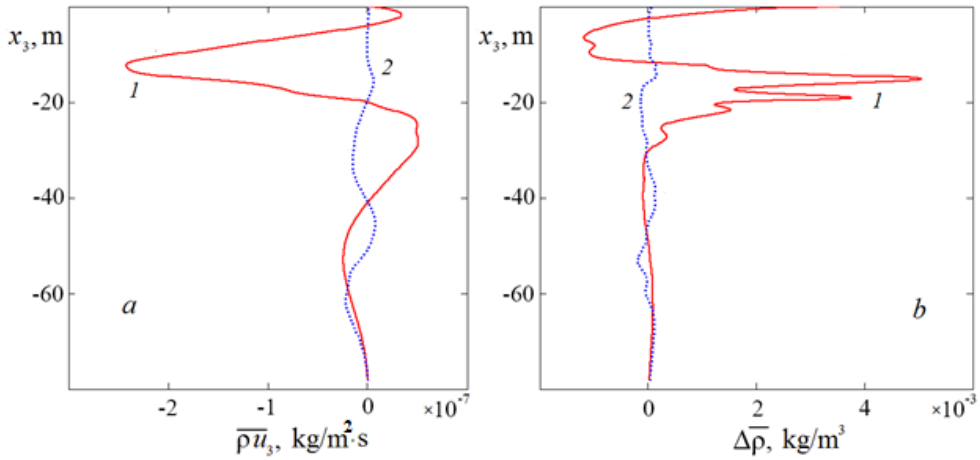

F i g. 5. Profiles of the vertical wave mass flux (*a*) and fine structure of density field (*b*) for the first (*1*) and second (*2*) modes of internal waves

Further we compare the wave fluxes and the generated fine structure of inertia-gravity internal waves of different frequencies. To do this, we consider the second mode with frequencies of 4, 1 and 12 cph at the same maximum wave amplitude of 0.5 m.

Figure 6, *a* shows vertical wave mass fluxes for waves of the indicated frequencies, and Fig. 6, *b* – profiles of the generated fine structure of the density field.

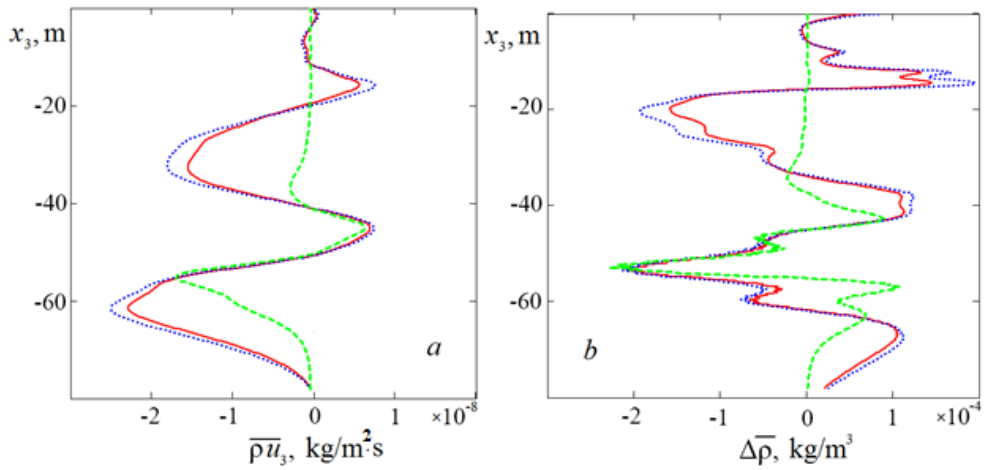

F i g. 6. Profiles of the vertical wave mass flux (*a*) and fine structure of density field (*b*) of the second mode for 15-minute internal waves (red curve), one-hour internal waves (blue curve) and 5-minute internal waves (green curve)

The vertical wave mass fluxes of the second mode of 15-minute, one-hour and 5-minute internal waves are co-directed and decrease in absolute value with the wave period decreasing. Fine-structure corrections to density for waves with 15-minute

and one-hour periods are close and only enhance the effect when summed up. The mentioned corrections do not introduce inversions into the vertical density distribution. A similar calculation was carried out for the first mode of internal waves. Fig. 7 shows the graphs of the vertical wave mass flux and generated fine density structure of the first-mode internal waves for 4, 1, and 12 cph frequencies.

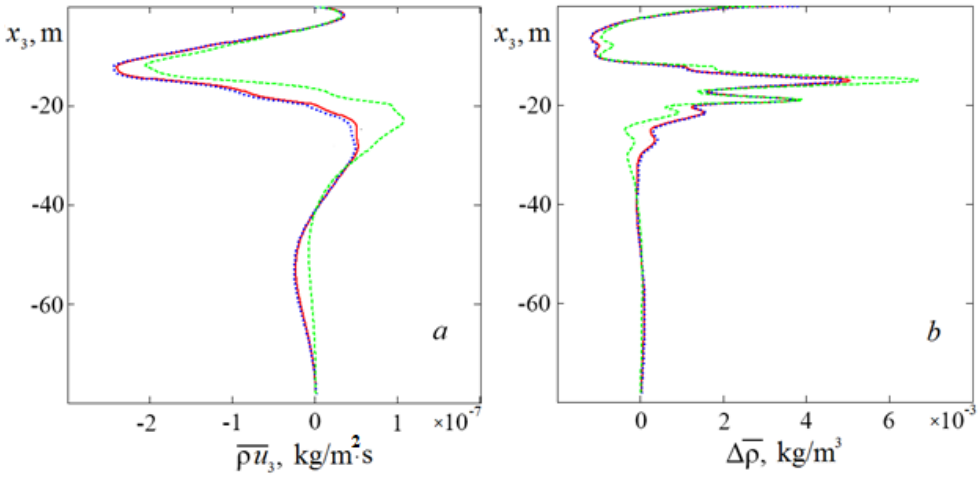

F i g. 7. Profiles of the vertical wave flux of mass (*a*) and fine structure of density field (*b*) of the first mode for 15-minute internal waves (red curve), one-hour internal waves (blue curve) and 5-minute internal waves (green curve)

In the first mode, the vertical wave mass fluxes and fine-structure corrections are almost the same for waves with 1 and 4 cph frequencies. They differ most noticeably in the pycnocline for waves with 12 cph frequency.

It is of interest to study the impact of horizontal inhomogeneity of the average density field on vertical wave mass fluxes and generated fine structure. In the horizontally homogeneous case, the terms containing horizontal gradients of the average density $\frac{\partial \rho_0}{\partial x}$ and $\frac{\partial \rho_0}{\partial y}$ are neglected in equation (4). Fig. 8 shows the dependence of the vertical wave mass fluxes and generated fine structure on the vertical coordinate for the second-mode internal waves with 4 cph frequency in the horizontally homogeneous and inhomogeneous cases with the same maximum wave amplitude of 0.5 m.

Thus, the amplitude of fine-structure oscillations and vertical wave mass fluxes in the horizontally inhomogeneous case are higher than in the homogeneous one.

Similar calculations were also performed for the first mode of internal waves. Fig. 9 shows the profiles of the vertical mass flux and generated fine structure for the first mode of internal waves with 4 cph frequency in the horizontally inhomogeneous and homogeneous cases.

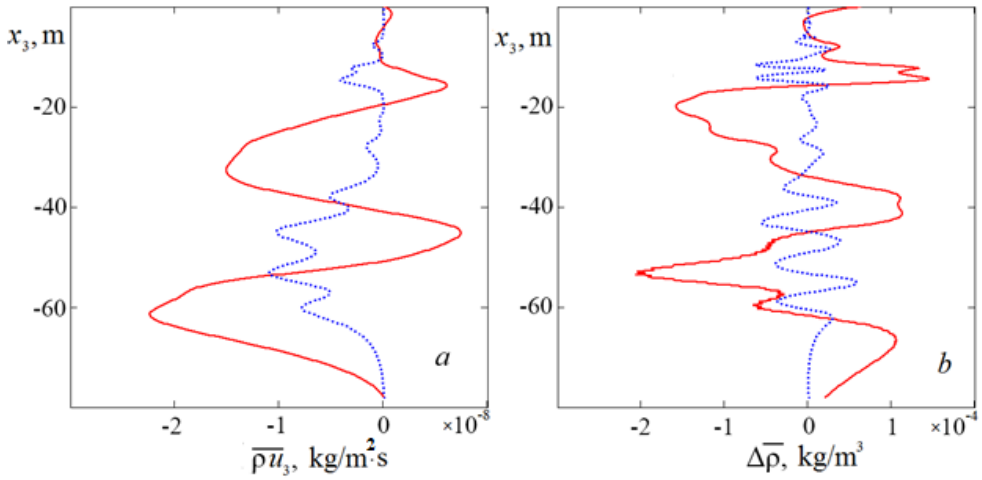

F i g. 8. Vertical distribution of the wave fluxes of mass (*a*) and generated fine structure (*b*) for the internal wave of the second mode in the horizontally inhomogeneous (red curve) and homogeneous (blue curve) cases

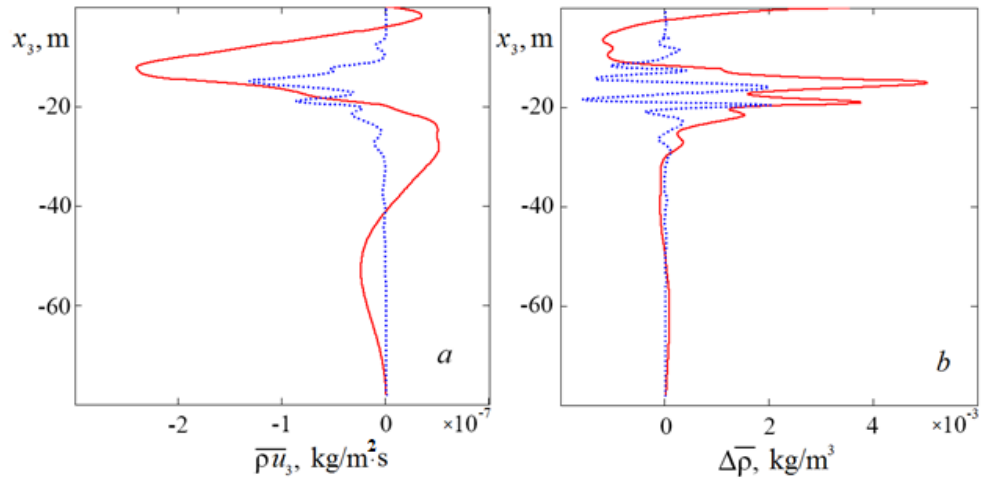

F i g. 9. Dependence on the vertical coordinate of the wave mass flux (*a*) and generated fine structure (*b*) for the internal wave of the second mode in the horizontally inhomogeneous (red curve) and homogeneous (blue curve) cases upon the vertical coordinate

Similarly, the first mode vertical wave mass fluxes and fine-structure correction to the density are higher in the case that is horizontally inhomogeneous in average density.

Conclusion

The paper presents a mechanism for generating vertical fine structure due to vertical wave mass fluxes. These fluxes are nonzero for the inertia-gravity internal waves in the presence of a flow in which the velocity component normal to the direction of wave propagation depends on the vertical coordinate. Unlike

previous works, we do not assume horizontal homogeneity of average density field. In contrast, the flow is assumed to be geostrophically balanced, i.e. vertical velocity shifts are balanced by the horizontal gradient of the average density field. This gradient is found from the "thermal wind" relations. It is shown that consideration of horizontal inhomogeneity of average density field increases both vertical wave mass fluxes and generated fine structure, the amplitude of fine-structure oscillations. The wave mass fluxes and fine-structure corrections to density are very close for waves of 1 and 4 cph frequencies, i.e. the overall effect only intensifies for waves of different frequencies.

REFERENCES

1. Chashechkin, Yu.D., 2022. Discrete and Continuous Symmetries of Stratified Flows past a Sphere. *Symmetry*, 14(6), 1278. https://doi.org/10.3390/sym14061278
2. Chashechkin, Yu.D., 2021. Foundations of Engineering Mathematics Applied for Fluid Flows. *Axioms*, 10(4), 286. https://doi.org/10.3390/axioms10040286
3. Chashechkin, Yu.D. and Ilinykh, A.Yu., 2023. Fine Structure of the Substance Distribution Pattern of a Free-Falling Drop on the Surface and in the Thickness of the Target Fluid in the Impact Mode of Merging. *Physical-Chemical Kinetics in Gas Dynamics*, 24(2), pp. 79-106. https://doi.org/10.33257/PhChGD.24.2.1043 (in Russian).
4. Gargett, A.E., 1976. An Investigation of the Occurrences of Oceanic Turbulence with Respect to Finestructure. *Journal of Physical Oceanography*, 6(2), pp. 139-156. https://doi.org/10.1175/1520-0485(1976)006<0139:AIOTOO>2.0.CO;2
5. Bell, T.H.Jr., 1974. Internal Wave-Turbulence Interpretation of Ocean Fine Structure. *Geophysical Research Letters*, 1(6), pp. 253-255. https://doi.org/10.1029/GL001i006p00253
6. Bagimov, I.S., Bulgakov, P.G., Korotaev, G.K., Panteleev, N.A. and Timchenko, A.N., 1978. Experimental Studies of the Temperature Field in the Seasonal Thermocline. In: MHI, 1978. *Marine Hydrophysical Research*. Sevastopol: MHI. Iss. 3, pp. 75-90 (in Russian).
7. Turner, J.S., 1981. *Buoyancy Effects in Fluids*. Cambridge Monographs on Mechanics. Cambridge, Great Britain: Cambridge University Press, 367 p. https://doi.org/10.1017/CBO9780511608827
8. Schmitt, R.W., 1981. Form of the Temperature-Salinity Relationship in the Central Water: Evidence for Double-Diffusive Mixing. *Journal of Physical Oceanography*, 11(7), pp. 1015-1026. https://doi.org/10.1175/1520-0485(1981)011<1015:FOTTSR>2.0.CO;2
9. Rudels, B., Björk, G., Muench, R.D. and Schauer, U., 1999. Double-Diffusive Layering in the Eurasian Basin of the Arctic Ocean. *Journal of Marine Systems*, 21(1-4), pp. 3-27. https://doi.org/10.1016/S0924-7963(99)00003-2
10. Zhurbas, V.M. and Lips, U.K., 1987. Discrimination of the Main Types of Thermohaline Fine Structure in the Ocean. *Oceanology*, 27(4), pp. 416-420.
11. Williams, A.J.3rd, 1974. Salt Fingers Observed in the Mediterranean Outflow. *Science*, 185(4155), pp. 941-943. https://doi.org/10.1126/science.185.4155.941
12. Pereskokov, A.I. and Fedorov, K.N., 1989. [Oxygenation of Ocean Thermocline Waters by Salt-Finger Convection]. *Transactions (Doklady) of the USSR Academy of Sciences. Earth Science Sections*, 309(1), pp. 241-244 (in Russian).
13. Pogrebnoi, A.E. and Panteleev, N.A., 2000. Convection of Salt Fingers in the C–SALT Region. *Physical Oceanography*, 10(3), pp. 215-232. https://doi.org/10.1007/BF02509220
14. Zhurbas, V.M., Kuzmina, N.P. and Kul'sha, O.E., 1987. Step-Like Stratification of the Ocean Thermocline Resulting from Transformations Associated with Thermohaline Salt Finger Intrusions (Numerical Experiment). *Oceanology*, 27(3), pp. 277-281.

15. Falina, A.S. and Volkov, I.I., 2003. On the Fine Structure and Thermohalinic Stability of the Abyssal Water in the Black Sea. *Oceanology*, 43(4), pp. 485-492.

16. Falina, A.S. and Volkov, I.I., 2005. Influence of Double Diffusion on the General Hydrological Structure of the Deep Waters in the Black Sea. *Oceanology*, 45(1), pp. 16-25.

17. Zhurbas, V.M. and Ozmidov, R.V., 1983. On the Internal Structure of the Fine Stepped Structure of the Main Ocean Thermocline. *Oceanology*, 23(6), pp. 938-943.

18. Rudels, B., Kuzmina, N., Schauer, U., Stipa, T. and Zhurbas, V., 2009. Double-Diffusive Convection and Interleaving in the Arctic Ocean – Distribution and Importance. *Geophysica,* 45(1-2), pp. 199-213.

19. Panteleev, N.A. and Okhotnikov, I.N., 2003. Intrusive Stratification of the Gulf-Stream Frontal Zone According to the Results of Investigations Performed during Cruise 43 of the R/V Akademik Vernadskii. *Physical Oceanography*, 13(2), pp. 104-115. https://doi.org/10.1023/A:1023748413882

20. Golovin, P.N., Antipov, N.N. and Klepikov, A.V., 2016. Intrusive Layering of the Antarctic Slope Front. *Oceanology*, 56(4), pp. 470-482. https://doi.org/10.1134/S0001437016030085

21. Kuzmina, N., Rudels, B., Zhurbas, V. and Stipa, T., 2011. On the Structure and Dynamical Features of Intrusive Layering in the Eurasian Basin in the Arctic Ocean. *Journal of Geophysical Research: Oceans*, 116(C8), C00D11. https://doi.org/10.1029/2010JC006920

22. Samodurov, A.S., 1993. Intrusion Layering and Vertical Diffusion in the Ocean Owing to Tidal Mixing at a Sloping Bottom. *Physical Oceanography*, 4(3), pp. 213-219. https://doi.org/10.1007/BF02197319

23. Samodurov, A.S., Lubitsky, A.A. and Panteleev, N.A., 1995. Contribution of Breaking Internal Waves to Structure Formation, Energy Dissipation, and Vertical Diffusion in the Ocean. *Physical Oceanography*, 6(3), pp. 177-190. https://doi.org/10.1007/BF02197516

24. Zatsepin, A.G., Golenko, N.N., Korzh, A.O., Kremenetskii, V.V., Paka, V.T., Poyarkov, S.G. and Stunzhas, P.A., 2007. Influence of the Dynamics of Currents on the Hydrophysical Structure of the Waters and the Vertical Exchange in the Active Layer of the Black Sea. *Oceanology*, 47(3), pp. 301-312. https://doi.org/10.1134/S0001437007030022

25. Podymov, O.I., Zatsepin, A.G. and Ostrovsky, A.G., 2017. Vertical Turbulent Exchange in the Black Sea Pycnocline and Its Relation to Water Dynamics. *Oceanology*, 57(4), pp. 492-504. https://doi.org/10.1134/S0001437017040142

26. Navrotsky, V.V., Izergin, V.L. and Lozovatsky, V.V., 2007. Internal Waves and Formation of Hydrophysical Fields Fine Structure in the Shelf Zone. *Far Eastern Seas of Russia*. Moscow: Nauka. Vol. 1, pp. 507-527 (in Russian).

27. Ivanov, V.A., Shul'ga, T.Ya., Bagaev, A.V., Medvedeva, A.V., Plastun, T.V., Verzhevskaia, L.V. and Svishcheva, I.A., 2019. Internal Waves on the Black Sea Shelf near the Heracles Peninsula: Modeling and Observation. *Physical Oceanography*, 26(4), pp. 288-304. https://doi.org/10.22449/1573-160X-2019-4-288-304

28. Leonov, A.I., Miropolsky, Yu.Z. and Tamsalu, R.E., 1977. Calculation of the Fine Structure of the Density and Velocity Fields as Exemplified by the Baltic Sea. *Oceanology*, 17(3), pp. 389-393.

29. Kistovich, A.V. and Chashechkin, Yu.D., 2007. Regular and Singular Components of Periodic Flows in the Fluid Interior. *Journal of Applied Mathematics and Mechanics*, 71(5), pp. 762-771. https://doi.org/10.1016/j.jappmathmech.2007.11.009

30. Chashechkin, Yu.D. and Ochirov, A.A., 2022. Periodic Waves and Ligaments on the Surface of a Viscous Exponentially Stratified Fluid in a Uniform Gravity Field. *Axioms*, 11(8), 402. https://doi.org/10.3390/axioms11080402

31. Kistovich, Y.V. and Chashechkin, Y.D., 1998. Linear Theory of the Propagation of Internal Wave Beams in an Arbitrarily Stratified Liquid. *Journal of Applied Mechanics and Technical Physics*, 39(5), pp. 729-737. https://doi.org/10.1007/bf02468043

32. LeBlond, P.H. and Mysak, L.A., 1978. *Waves in the Ocean*. Amsterdam; New York: Elsevier Scientific Publishing Company, 602 p.

33. LeBlond, P.H., 1966. On the Damping of Internal Gravity Waves in a Continuously Stratified Ocean. *Journal of Fluid Mechanics*, 25(1), pp. 121-142. https://doi.org/10.1017/S0022112066000089

34. Slepyshev, A.A., 2016. Vertical Momentum Transfer by Internal Waves When Eddy Viscosity and Diffusion Are Taken into Account. *Izvestiya, Atmospheric and Oceanic Physics*, 52(3), pp. 301-308. https://doi.org/10.1134/S0001433816030117

35. Slepyshev, A.A., 2022. Vertical Momentum Transfer Induced by Internal Inertial-Gravity Waves in Flow with Account of Turbulent Viscosity and Diffusion. *Fluid Dynamics*, 57(2), pp. 183-192. https://doi.org/10.1134/S0015462822020094

36. Slepyshev, A.A. and Nosova, A.V., 2022. Vertical Transfer of Momentum by Internal Waves in the Western Part of the Mediterranean Sea. *Physical Oceanography*, 29(4), pp. 334-346.

37. Slepyshev, A.A. and Nosova, A.V., 2020. Generation of Vertical Fine Structure by the Internal Waves with the Regard for Turbulent Viscosity and Diffusion. *Physical Oceanography*, 27(1), pp. 3-17. https://doi.org/10.22449/1573-160X-2020-1-3-17

38. Slepyshev, A.A., 2022. Vertical Momentum Transfer by Internal Waves in a Shear Flow Taking into Account Turbulent Viscosity and Diffusion. *Izvestiya, Atmospheric and Oceanic Physics*, 58(5), pp. 433-439. https://doi.org/10.1134/S0001433822050115

39. Slepyshev, A.A. and Vorotnikov, D.I., 2019. Generation of Vertical Fine Structure by Internal Waves in a Shear Flow. *Open Journal of Fluid Dynamics*, 9(2), pp. 140-157. https://doi.org/10.4236/ojfd.2019.92010

40. Ankudinov, N.O. and Slepyshev, A.A., 2021. Vertical Momentum Transfer Induced by Internal Waves in a Two-Dimensional Flow. *Fluid Dynamics*, 56(3), pp. 343-352. https://doi.org/10.1134/S0015462821030022

41. Slepyshev, A.A. and Vorotnikov, D.I., 2017. Vertical Transport of Momentum by the Inertial-Gravity Internal Waves in a Baroclinic Current. *Physical Oceanography,* (4), pp. 3-15. https://doi.org/10.22449/1573-160X-2017-4-3-15

42. Slepyshev, A.A., 2021. Vertical Transfer of Momentum by Inertia-Gravity Internal Waves on a Two-Dimensional Shear Flow. *Physical Oceanography*, 28(4), pp. 363-375. https://doi.org/10.22449/1573-160X-2021-4-363-375

43. Vorotnikov, D.I. and Slepyshev, A.A., 2018. Vertical Momentum Fluxes Induced by Weakly Nonlinear Internal Waves on the Shelf. *Fluid Dynamics*, 53(1), pp. 21-33. https://doi.org/10.1134/S0015462818010160

44. Slepyshev, A.A. and Laktionova, N.V., 2019. Vertical Transport of Momentum by Internal Waves in a Shear Current. *Izvestiya, Atmospheric and Oceanic Physics*, 55(6), pp. 662-668. https://doi.org/10.1134/S0001433819060148

45. Jones, W.L., 1967. Propagation of Internal Gravity Waves in Fluids with Shear Flow and Rotation. *Journal of Fluid Mechanics*, 30(3), pp. 439-448. https://doi.org/10.1017/S0022112067001521

46. Bulatov, V.V. and Vladimirov, Yu.V., 2020. Dynamics of Internal Gravity Waves in the Ocean with Shear Flows. *Russian Journal of Earth Sciences*, 20(4), ES4004. https://doi.org/10.2205/2020ES000732

47. Bulatov, V.V. and Vladimirov, I.Yu., 2022. Internal Gravity Waves Generated by an Oscillating Disturbance Source in a Stratified Medium in the Presence of Two-Dimensional Shear Flows. *Fluid Dynamics*, 57(4), pp. 477-485. https://doi.org/10.1134/s0015462822040012

48. Longuet-Higgins, M.S., 1969. On the Transport of Mass by Time Varying Ocean Current. *Deep Sea Research and Oceanographic Abstracts*, 16(5), pp. 431-447. https://doi.org/10.1016/0011-7471(69)90031-X

Submitted 05.09.2023; approved after review 25.12.2023;
accepted for publication 18.01.2024.

About the authors:

Aleksandr A. Slepyshev, Leading Research Associate, Marine Hydrophysical Institute of RAS (2 Kapitanskaya Str., Sevastopol, 299011, Russian Federation), DSc (Phys.-Math.), **ResearcherID: V-6948-2017**, **ORCID ID: 0000-0002-9259-7558**, slep55@mail.ru

Nikita O. Ankudinov, Leading Engineer-Researcher, Marine Hydrophysical Institute of RAS (2 Kapitanskaya Str., Sevastopol, 299011, Russian Federation), ankudinff@gmail.ru

Contribution of the co-authors:

Aleksandr A. Slepyshev – problem statement, theoretical part of the work: mathematical formulation of the model, derivation of all formulas

Nikita O. Ankudinov – numerical calculations using the proposed model, graphical presentation of the results

The authors have read and approved the final manuscript.

The authors declare that they have no conflict of interest.